

1  
2  
3  
4  
5  
6  
7  
8  
9  
10  
11  
12  
13  
14  
15  
16  
17  
18  
19  
20  
21

**Application of positive matrix factor analysis in heterogeneous  
kinetics studies: An improvement to the mixed-phase relative  
rates technique**

Y. Liu, S.-M. Li and J. Liggio\*

Air Quality Processes Research Section, Environment Canada, Toronto, M3H  
5T4, Canada

---

\*Corresponding author. Phone: 1-416-739-4840; fax: 1-416-739-4281;  
E-mail: [John.Liggio@ec.gc.ca](mailto:John.Liggio@ec.gc.ca)

22 **Abstract:**

23 The mixed-phase relative rate approach for determining aerosol particle organic  
24 heterogeneous reaction kinetics is often performed utilizing mass spectral tracers as a  
25 proxy for particle phase reactant concentration. However, this approach may be  
26 influenced by signal contamination from oxidation products during the experiment. In  
27 the current study, the mixed-phase relative rates technique has been improved by  
28 combining a Positive Matrix Factor (PMF) analysis with electron ionization Aerosol  
29 Mass Spectrometry, thereby removing the influence of m/z fragments from reaction  
30 products on the reactant signals. To demonstrate the advantages of this approach, the  
31 heterogeneous reaction between OH radicals and citric acid (CA) was investigated  
32 using a photochemical flow tube coupled to a compact time-of-flight aerosol mass  
33 spectrometer (C-ToF-AMS). The measured heterogeneous rate constant ( $k_2$ ) of citric  
34 acid toward OH was  $(3.31 \pm 0.29) \times 10^{-12} \text{ cm}^3 \text{ molecule}^{-1} \text{ s}^{-1}$  at 298 K and (30 $\pm$ 3) % RH  
35 and was **several** times greater than **the** results utilizing individual m/z fragments. This  
36 phenomenon was further evaluated for particulate-phase organophosphates (TPhP,  
37 TDCPP, and TEHP), leading to  $k_2$  values significantly larger than previously reported.  
38 The results suggest that heterogeneous kinetics can be significantly underestimated  
39 **when the structure of the products is highly similar to the reactant and when a**  
40 **non-molecular tracer is measured with a unit mass resolution aerosol mass**  
41 **spectrometer.** The results also suggest that the heterogeneous lifetime of organic  
42 aerosol in models can be overestimated due to underestimated OH uptake coefficients.  
43 **Finally, a comparison of reported rate constants implies that the heterogeneous**

44 oxidation of aerosols will be dependent upon a number of factors related to the  
45 reaction system, and that a single rate constant for one system cannot be universally  
46 applied under all conditions.

47

48

49

50

51

52

53

54

55

56

57

58

59

60

61

62

63

64

65

## 66 **1. Introduction**

67       Reaction kinetics data provide key parameters for both air quality and climate  
68 models. They are required to compute the trace gas and particle matter (PM) content  
69 of the atmosphere (Kolb et al., 2010) and to evaluate the atmospheric lifetime and fate  
70 for individual species. Organic particle makes up 10-90 % of the global submicron  
71 particle mass in the lower troposphere (Zhang et al., 2011), and is comprised of  
72 various reactive organic species, which are subject to atmospheric heterogeneous  
73 oxidation. Previous studies have found that heterogeneous reactions with OH in  
74 particular, can lead to an increase in density, CCN activation (George and Abbatt,  
75 2010) and optical extinction (Cappa et al., 2011) of organic particulate matter.  
76 Therefore, there is a growing interest in understanding not only the mechanism of PM  
77 transformation through heterogeneous reactions including oxidation, but also  
78 determining the rates at which organic aerosols are chemically transformed in the  
79 atmosphere.

80       To this end, Donahue et al. (2005) and Hearn and Smith (2006) developed a  
81 mixed-phase relative rate technique for measuring organic PM component  
82 heterogeneous reaction kinetic rate constants. In this method, the rate constant of the  
83 compound of interest is determined from the decrease of its particle phase relative  
84 concentration as a function of oxidant exposure. The oxidant levels are  
85 simultaneously estimated via the measured loss of a gas phase reference compound  
86 after applying the known second-order rate constant ( $k_2$ ) toward the oxidant. In this  
87 approach the rates of chemical change are given by,

88 
$$-\frac{dc_A}{dt} = k_{2,A}c_Ac_{Ox} \quad (1)$$

89 
$$-\frac{dc_R}{dt} = k_{2,R}c_Rc_{Ox} \quad (2)$$

90 where  $c_A$ ,  $c_R$  and  $c_{Ox}$  are the particle phase concentration of the compound of interest  
 91 (A), the gas phase concentration of the reference compound (R) and oxidant  
 92 (molecules  $\text{cm}^{-3}$ ) respectively, while  $k_{2,A}$  and  $k_{2,R}$  are the second-order rate constant of  
 93 A and R to the oxidant ( $\text{cm}^3 \text{ molecule}^{-1} \text{ s}^{-1}$ ). A relative rate constant ( $k_r$ ) (ie: particle  
 94 phase reaction rate of A, relative to the gas phase rate of R) can be derived by dividing  
 95 Eq. (1) by Eq. (2). The derivation of  $k_r$  provides a means to obtain heterogeneous  
 96 kinetic data without the need to know the absolute concentration of the oxidant. The  
 97 differential and integral forms for the relative rates technique are shown as Eq. (3) and  
 98 (4),

99 
$$\frac{dc_A}{c_A} = \frac{k_{2,A}}{k_{2,R}} \frac{dc_R}{c_R} = k_r \frac{dc_R}{c_R} \quad (3)$$

100 
$$\log \frac{c_A}{c_{A,0}} = k_r \log \frac{c_R}{c_{R,0}} \quad (4)$$

101 from which the relative rate constant ( $k_r$ ), is the slope of the line derived by plotting  
 102 the logarithmic relative concentration of A against that of R (relative to initial  
 103 conditions;  $C_{A,0}$ ). The second-order heterogeneous rate constant of the compound of  
 104 interest ( $k_{2,A}$ ) towards the oxidant may then be calculated using the obtained  $k_r$  and the  
 105 known  $k_{2,R}$  (ie:  $k_{2,A} = k_r \times k_{2,R}$ ).

106 Using this method, a number of studies have quantified the uptake coefficients of  
 107  $\text{O}_3$ , OH, Cl, and  $\text{NO}_3$  on various organic particles, and the corresponding second order  
 108 rate constants for the degradation of organic compounds (Hearn and Smith,  
 109 2006; George et al., 2007; Lambe et al., 2007; McNeill et al., 2007; McNeill et al.,

110 2008;Smith et al., 2009;Kessler et al., 2010;Renbaum and Smith, 2011;Kessler et al.,  
111 2012;Liu et al., 2012;Sareen et al., 2013).

112 Although gas chromatograph mass spectrometry (GC-MS) was widely used in the  
113 kinetics studies (Weitkamp et al., 2008a;Weitkamp et al., 2008b;Lambe et al.,  
114 2009;Isaacman et al., 2012), quantifying the particle phase loss of an organic  
115 compound in such studies often relies upon aerosol mass spectrometry techniques to  
116 monitor specific particle phase reactant ions of interest in semi-real time. Aerosol  
117 mass spectrometry instruments utilizing high resolution detector and soft ionization  
118 techniques, such as chemical ionization (Aerosol CIMS) (Hearn and Smith,  
119 2006;McNeill et al., 2007;McNeill et al., 2008;Renbaum and Smith, 2011;Sareen et  
120 al., 2013) and vacuum ultraviolet photo-ionization (VUV-ATOFMS)(Liu et al., 2012),  
121 have been utilized to measure the concentration of the target organic compounds in  
122 particles. However, Aerosol Time-of-Flight or Quadrupole Mass Spectrometry  
123 (ToF-AMS or Q-AMS) employing electronic ionization (EI; 70 eV) as an ion source  
124 remains the prevalent instrument used in such organic particle experiments. In  
125 utilizing this approach, a specific fragment is often chosen as a tracer for the particle  
126 phase compound of interest. For example, m/z 297 has been selected as a tracer for  
127 bis(2-ethylhexyl) sebacate (BES) (George et al., 2007), m/z 71 for hexacosane  
128 (Lambe et al., 2007), m/z 113 for squalane (Smith et al., 2009), m/z 104 and 144 for  
129 erythritol and levoglucosan (Kessler et al., 2010), and m/z 152, 68 and 98 for  
130 1,2,3,4-butanetetracarboxylic acid, citric acid and tartaric acid (Kessler et al., 2012)  
131 respectively.

132        However, the use of EI in conjunction with a particle vaporizer in the AMS  
133 results in heavy fragmentation for organic compounds due to the high energy  
134 associated with the EI source (70 eV) and the high temperature (~873 K) of the  
135 vaporizer (Jayne et al., 2000; Allan et al., 2003). Under such conditions, the tracer m/z  
136 fragment is prone to interferences due to (1) the fragmentation of larger ions and/or  
137 molecules and (2) fragments from particle phase oxidation products. Both can  
138 contribute to the tracer m/z signal, leading to an insensitive or nonlinear response of  
139 the tracer m/z to the concentration of the target reactant during oxidation. The same  
140 may also be true for the m/z for the molecular ion should one exist. **In particular, it is**  
141 **true if the structure of the product is highly similar to the reactant and when the tracer**  
142 **is measured with a unit-mass resolution (UMR) aerosol mass spectrometer.** Although  
143 it is often assumed that the chosen tracer ion does not contribute significantly to the  
144 mass spectra of any possible oxidation products or vice versa (Kessler et al., 2010),  
145 this is not always the case. In our previous work, we observed that the magnitude of  
146 the second order heterogeneous rate constant ( $k_2$ ) increases as a function of increasing  
147 m/z of the fragment chosen as a tracer of the parent molecule (Liu et al., 2014). **The**  
148 **same trend has also been observed for the OH oxidation of ambient biogenic**  
149 **secondary organic aerosol (SOA) (Slowik et al., 2012).** This suggests an interference  
150 from the fragments selected, and points to the necessity to separate the signals of the  
151 compound of interest, from other compounds (products and/or fragment) for kinetic  
152 studies.

153        In the current study, we improve the mixed-phase relative rate technique used for

154 studies of the heterogeneous oxidation of organic aerosol (OA) using positive matrix  
155 factorization (PMF) analysis of AMS derived kinetic data. Heterogeneous kinetics of  
156 citric acid (CA) toward OH oxidation was studied in a photo-chemical flow tube  
157 coupled to an Aerodyne C-ToF-AMS and an Ionicon Analytik High Resolution Proton  
158 Transfer Reaction Mass Spectrometer (PTR-ToF-MS). As it was applied to  
159 heterogeneous oxidation of ambient biogenic SOA (Slowik et al., 2012), PMF  
160 analysis was used to successfully deconvolve the full mass spectra of the reactant  
161 from the potential oxidation products, hence allowing proper accounting of the time  
162 evolution of reactant concentrations during photochemical oxidation.

## 163 **2. EXPERIMENTAL DETAILS**

164 **2.1 Flow tube experiments.** A detailed schematic representation of the experimental  
165 system utilized in this study has been described elsewhere (Liu et al., 2014). Briefly,  
166 organic particles (citric acid) were generated via atomization (model 3706, TSI), dried  
167 through a diffusion drier and size-selected with a differential mobility analyzer (DMA)  
168 (model 3081, TSI). The dried, monodispersed CA particles were introduced into the  
169 flow tube reactor and exposed to differing OH concentrations. OH radicals were  
170 produced by the photolysis of O<sub>3</sub> at 254 nm in the presence of water vapor. O<sub>3</sub> was  
171 generated by passing zero air through an O<sub>3</sub> generator (OG-1, PCI Ozone Corp.). The  
172 O<sub>3</sub> concentration in the reactor was measured using an O<sub>3</sub> monitor (model 205, 2B  
173 Technologies) and ranged from 0-1000 ppbv. Relative humidity (RH) in the reactor  
174 was held constant (30±3) % by varying the ratio of wet to dry air used as an air source,  
175 and was measured at the exit of the flow tube reactor. The temperature was held



176 constant at 298 K by circulating a temperature controlled fluid through the outer  
177 jacket of the reactor. **The residence time in the flow reactor was 52 s.** The steady-state  
178 OH exposures were varied from 0 to  $\sim 7.0 \times 10^{11}$  molecules  $\text{cm}^{-3}$  s which was estimated  
179 on the basis of the decay of methanol from (as a reference compound) its reaction  
180 with OH. The decay of methanol from its reaction with OH was measured using the  
181 PTR-ToF-MS. The  $k_2$  of methanol,  $9.4 \times 10^{-13}$   $\text{cm}^3$  molecule $^{-1}$  s $^{-1}$ , was used for the OH  
182 exposure calculation (Atkinson and Arey, 2003).

183 OH radical reactions were performed in a custom-made reactor consisting of two  
184 electro-polished stainless steel cylinders with inner diameter of 7.3 cm. The first stage  
185 contained static mixing elements (StaMixCo) to ensure that particles and gas phase  
186 species were well mixed prior to entering the reaction region (second stage). Fluid  
187 dynamics simulations of the flow tube confirmed that particles and gas phase species  
188 were well mixed in the reactor, with a uniform initial velocity profile. The size and  
189 composition of the particles exiting the reactor were measured by a scanning mobility  
190 particle sizer (SMPS, TSI) and an Aerodyne C-ToF-AMS (Drewnick et al., 2005)

191 Control experiments demonstrated that O<sub>3</sub> or 254 nm light exposure did not lead  
192 to the decomposition of CA. Analytic grade CA (EM, Germany) was used as received.

193 18.2 MΩ water was used as solvent.

## 194 **2.2 PMF analysis and kinetics calculation.**

195 PMF is a multivariate factor analysis tool that decomposes a matrix of speciated  
196 sample data into two matrices, namely, factor contributions and factor profiles  
197 (Paatero and Tapper, 1994), such that

198  $x_{ij} = \sum_p g_{ip} f_{pj} + e_{ij}$  (5)

199 Where  $i$  and  $j$  refer to row and column indices in the matrix, respectively,  $p$  is the  
200 number of factors in the solution,  $x_{ij}$  is an element of the  $m \times n$  matrix  $X$  of measured  
201 data elements to be fit, and  $e_{ij}$  is the residual. Results are constrained so that no  
202 sample can have a negative source contribution. The PMF solution minimizes the  
203 object function  $Q$  (Eq.6), based upon the uncertainties ( $u$ ) (Norris and Vedantham,  
204 2008).

205  $Q = \sum_{i=1}^n \sum_{j=1}^m \left( \frac{e_{ij}}{u_{ij}} \right)^2$  (6)

206 Its ability to separate the signals of a multi-component matrix has been well  
207 established. PMF analysis has been widely used for source apportionment of ambient  
208 particles in field measurements (Song et al., 2006; Yuan et al., 2006; Viana et al.,  
209 2008; Ulbrich et al., 2009; Liggiio et al., 2010; Schwartz et al., 2010). Three secondary  
210 organic aerosol factors (SOA1, SOA2, SOA3) have been identified for OH initiated  
211 oxidation of laboratory SOA (George and Abbatt, 2010). **Similarly, SOA factors have**  
212 **also been successfully isolated in OH oxidation of ambient biogenic SOA (Slowik et**  
213 **al., 2012).** Therefore, the use of PMF for separating the reactants from the products in  
214 laboratory studies aimed at using the relative rates method for heterogeneous kinetic  
215 studies would seem to be a reasonable approach.

216 The AMS data for CA oxidation from all experiments combined were used as  
217 input into the PMF Evaluation Toolkit (PET) v2.05 (Paatero, 1997; Paatero and Tapper,  
218 1994) to separate the signals of CA and the corresponding oxidation products. In the  
219 AMS data, the  $m$  rows of  $X$  are ensemble average mass spectra (MS) of typically tens

220 of thousands of particles measured over each averaging period (typically 2 min) and  
221 the  $n$  columns of  $X$  are the time series (TS) of each  $m/z$  sampled.

222 PMF analyses were done in the robust mode. The default convergence criteria  
223 were not modified. The  $Q$  values as a function of FPEAK from -1 to +1 were  
224 examined (Reff et al., 2007). For the variables with signal-to-noise ratio (SNR) less  
225 than 0.2 (“bad” variables) and downweight variables with SNR between 0.2 and 2  
226 (“weak” variables), their error estimates were increased by a factor of 10 and 3,  
227 respectively, as recommended by Paatero and Hopke (Paatero and Hopke, 2003). In  
228 this study, the SNR of all  $m/z$  fragments are larger than 0.2. The error values for  $m/z$   
229 44, 18, 17 and 16 were multiplied by  $\sqrt{4}$ .

230 The extracted factor profiles (mass spectra for CA and the oxidation products)  
231 were compared with the NIST mass spectrum of pure CA and that measured with the  
232 C-ToF-AMS directly via atomization. The temporal concentration profiles (factor  
233 contributions) of CA were further confirmed via comparison to the known  
234 experimental conditions used for kinetics calculations (ie: zero OH exposure should  
235 result in a CA factor contribution of 100 %). For comparison with the PMF results,  
236 the kinetic rate constants ( $k_r$ ) were also calculated using specific individual tracers of  
237 CA at  $m/z$  87, 129 and 147, separately. The  $k_r$  of CA toward methanol was calculated  
238 according to Eq. (4). The  $k_2$  of CA was further calculated with the known  $k_2$  of  
239 methanol and  $k_r$ .

240 The reactive uptake coefficient of OH ( $\gamma_{OH}$ ) with CA was calculated using the  
241 following formulation (Kessler et al., 2010; Worsnop et al., 2002; Kessler et al.,

242 2012;Liu et al., 2012):

$$243 \gamma_{\text{OH}} = \frac{2D_p \rho_{\text{CA}} N_A}{3v_{\text{OH}} M_{\text{CA}}} k_2 \quad \text{Eq (7)}$$

244 Where  $D_p$  is the surface-weight average particle diameter of unreacted particles (cm),

245  $\rho_{\text{CA}}$  is the density of CA ( $\text{g cm}^{-3}$ ),  $N_A$  is Avogadro's number,  $v_{\text{OH}}$  is the average speed

246 of OH radicals in the gas phase ( $\text{cm s}^{-1}$ ),  $M_{\text{CA}}$  is the molecular weight of CA ( $\text{g mol}^{-1}$ ).

247

## 248 **3.0 Results**

### 249 **3.1 PMF analysis of AMS data.**

250 To ensure that oxidation of CA in particles does not result in a PTR-ToF-MS

251 response for methanol in the gas phase (thus compromising the OH radical reference

252 measurement), the oxidation of pure CA was performed in the absence of methanol,

253 with no gas phase methanol signal detected by the PTR-ToF-MS. The mass

254 concentration of the OA measured with the AMS during oxidation is shown in Figure

255 1A, which was constant. The results of Figure 1A demonstrate that the aerosol source

256 is adequately stable for kinetic studies to be performed.

257 A two factor solution from the PMF analysis accounts for **99.98** % of the

258 variance of the data. When the number of factors is greater than 2, none of the

259 obtained factors resembles that of pure CA, whose contribution should be

260 approximately 100 % when OH is absent in the reactor. Figures 1B and C represent

261 the temporal variations of the typical 2-factor PMF solution of AMS data when CA is

262 exposed to varying OH concentrations. The error bars indicate the rotational

263 uncertainty in the PMF analysis. Three independent experiments were performed to

264 test the response of CA signal to OH exposure (determined by O<sub>3</sub> concentration). In  
265 the first and the third experiments, OH exposure was stepped downwards (high to low  
266 OH) by changing the power of O<sub>3</sub>-generator with the same flow rate and RH, while  
267 the inverse sequence was performed in the second experiment.

268 As demonstrated in Figure 1B and C, in the absence of OH radical (labeled“0”),  
269 factor 1 (Figure 1B) accounts for (94.7±0.9) % of the OA mass, while factor 2 (Figure  
270 1C) contributes (6.2±0.7) % of OA. This is consistent with the experimental  
271 conditions of zero OH radical (ie: no oxidation), and suggests that factor 1 should be  
272 assigned to the citric acid reactant. Impurities in the CA or the water used to atomize  
273 CA likely contributed to factor 2. When OH exposure was decreased in a step-wise  
274 manner in the first and the third experiment (Figure 1B), the extracted factor  
275 representative of CA (factor 1) increased synchronously, and is accompanied with a  
276 decrease in factor 2. Therefore, factor 2 is interpreted as the OH oxidation products of  
277 CA. This is consistent with the second experiment, where the inverse trend was  
278 observed with a step-wise OH exposure increase. Based upon this evidence, we  
279 conclude that changes in the time series of factors 1 and 2 extracted by PMF are  
280 consistent with the expected response to OH exposures, namely, that higher OH  
281 exposure resulted in a decrease in CA (factor 1) and an increase in the oxidation  
282 products (factor 2).

283 The factor profiles (ie: mass spectra) extracted by PMF analysis are shown in  
284 Figure 2. The main fragments of CA including m/z values 129 (C<sub>5</sub>H<sub>5</sub>O<sub>4</sub><sup>+</sup>) and 87  
285 (C<sub>3</sub>H<sub>3</sub>O<sub>3</sub><sup>+</sup>) are present in factor 1 (Figure 2A). These fragments are in good agreement

286 with the NIST mass spectra of pure CA and the mass spectrum of pure CA particles  
287 measured with the C-ToF-AMS (Figure 3). Figure 4 further compared the normalized  
288 mass spectra of factor 1 and pure CA directly measured with the C-ToF-AMS. The  
289 relative intensities for all ions of pure CA are linearly correlated with that of factor 1  
290 with a slope of 0.985 and R of 0.9999. This further confirmed that factor 1 should be  
291 assigned to unreacted CA. Figure 2C shows the difference mass spectra (factor 2 –  
292 factor 1). Consumption of m/z values 147 ( $C_5H_7O_5^+$ ), 129, 87, 85 ( $C_4H_5O_2^+$ ), 68  
293 ( $C_4H_4O^+$ ) and 60 ( $C_2H_4O_2^+$ ) can be observed, which is consistent with the assignment  
294 that factor 2 belongs to oxidation products of CA. However, small changes in the  
295 relative intensities of these peaks suggest that the structure of the oxidation products  
296 of CA are likely similar to that of CA. For example, as shown in Figure 2A and B, the  
297 intensity of m/z 129 and 87 in factor 2 are  $0.0125 \pm 0.0046$  and  $0.0218 \pm 0.0013$   
298 compared to  $0.0141 \pm 0.0046$  and  $0.0235 \pm 0.0013$  in factor 1.

299 The changes of the relative concentrations of gas phase methanol and particle  
300 phase CA are shown in Figure 5. The signal of CA extracted by PMF analysis also  
301 responded to OH exposure as expected, when methanol was present in the gas phase,  
302 which is similar to that of Figure 1. The relative intensities of the typical tracers of CA  
303 at m/z 87, 129 and 147 are shown in Figure 5C. However, the relative loss of these  
304 tracers as a function of OH exposure in Figure 5C is much smaller than that of the CA  
305 factor derived from the PMF analysis (Figure 5B). In addition, the consumption of the  
306 smaller tracer (m/z 87) is substantially lower than that of the larger ones (m/z values  
307 129 and 147). For example, the maximum consumption of CA extracted with PMF

308 analysis is approximately 80 %, in comparison to ~30 %, ~10 % and 5 % for m/z  
309 values 147, 129 and 87, respectively. These results support the small differences in the  
310 mass spectra between the unreacted CA and its oxidation products as shown in Figure  
311 2. Furthermore, it suggests that the measured loss of these fragments, which were  
312 supposedly only derived from CA, had in fact contributions from the fragmentation of  
313 the products of CA oxidation. This ultimately would lead to an underestimation of the  
314 second order heterogeneous rate constant (or OH uptake coefficients) if these  
315 fragments were chosen as the proxies for the particle phase concentration of CA.

316 **3.2 Reaction kinetics.** The saturation vapor pressure of CA at 298K is  $1.6 \times 10^{-7}$  Pa  
317 (Huisman et al., 2013), thus 99.9% of CA should be present in the particle phase  
318 under the current experimental conditions according to a partition model (Kroll and  
319 Seinfeld, 2008; Pankow, 1994). Although new particle formation was observed with a  
320 CPC in the experiments (at the exit of the reactor), it has no influence on the measured  
321 mass concentration of OA due to the small particle size of the new particles. This is  
322 well supported by the constant mass concentration of OA measured with the AMS  
323 during oxidation experiments (Figure 1A). In addition, as pointed out in our previous  
324 work (Liu et al., 2014), evaporation of CA from particles could potentially contribute  
325 to the decreases in particle phase CA concentration observed as a function of OH  
326 exposure. If CA evaporation was at play, the derived reaction rates will be  
327 overestimated using either the present approach or the simpler methods of using  
328 single fragments. The evaporation of CA from the particle phase under these  
329 experimental conditions from control experiments is less than 0.005 % based upon an

330 evaporation model (Jacobson, 2005). This implies that the observed changes in CA  
331 concentration in the particle phase were due to the particle phase reaction.

332 The relative rates (relative to initial conditions) for CA and methanol in these  
333 experiments are shown in Figure 6. The logarithmic  $c/c_0$  of CA both measured with  
334 the tracers and extracted with PMF analysis linearly correlated to that of methanol  
335 with  $R^2 > 0.95$ . The derived relative rate constant based upon PMF analysis is  
336  $3.01 \pm 0.27$ , while it is  $0.72 \pm 0.05$  and  $0.22 \pm 0.01$  for  $m/z$  values 147 and 129,  
337 respectively. Applying the  $k_2$  value of methanol towards OH of  $9.4 \times 10^{-13} \text{ cm}^3$   
338  $\text{molecule}^{-1} \text{ s}^{-1}$  at 298 K (Atkinson and Arey, 2003), the  $k_2$  of CA is calculated as  
339  $(2.83 \pm 0.25) \times 10^{-12}$  using the PMF approach, or  $(6.77 \pm 0.47) \times 10^{-13}$  using the single  
340 tracer at  $m/z$  147 and  $(2.02 \pm 0.01) \times 10^{-13} \text{ cm}^3 \text{ molecule}^{-1} \text{ s}^{-1}$  using the single tracer at  
341  $m/z$  129, respectively. The reaction between methanol and OH radicals occurs in the  
342 gas phase, while for the CA oxidation it occurs in particle phase. Thus it is necessary  
343 to correct for OH diffusion from the bulk gas phase to the particle phase. Applying a  
344 diffusion correction utilizing a previously developed empirical formula (Fuchs and  
345 Sutugin, 1970; Worsnop et al., 2002; Widmann and Davis, 1997), the  
346 diffusion-corrected  $k_2$  is  $(3.31 \pm 0.29) \times 10^{-12}$  using the PMF approach, and  
347  $(7.92 \pm 0.55) \times 10^{-13}$  and  $(2.36 \pm 0.01) \times 10^{-13} \text{ cm}^3 \text{ molecule}^{-1} \text{ s}^{-1}$  using single tracers at  $m/z$   
348 147 and 129, respectively. The diffusion-corrected  $\gamma_{\text{OH}}$  is calculated as  $2.74 \pm 0.24$   
349 using the PMF approach, and  $0.66 \pm 0.46$  and  $0.20 \pm 0.01$  using single tracers at  $m/z$  147  
350 and 129, respectively.

351 **It should be pointed out that oxidant diffusion in the particle phase should lead to**



352 a concentration gradient of oxidant and a negative impact on reaction kinetics  
353 (Donahue et al., 2005). However, as shown in Figure 6, this effect is negligible under  
354 the current experimental conditions. Based upon the measured  $c/c_0$  and the initial  
355 diameter of the CA particles, the maximum OH diffusion depth is approximately 25  
356 nm. Given the residence time ( $\tau$ ) in this study (52 s), a significant OH concentration  
357 gradient will exist in particle phase if the  $D_{OH}$  in CA particles is smaller than  $1.2 \times 10^{-17}$   
358  $m^2 s^{-1}$  ( $D=l^2/\tau$ ) (Donahue et al., 2005). At the present time, the  $D_{OH}$  in CA particles is  
359 unavailable. However, Price et al. (Price et al., 2014) have reported the diffusion of  
360  $D_2O$  in several organics (sucrose and levoglucosan) to be larger than  $\sim 1 \times 10^{-16} m^2 s^{-1}$   
361 even under dry condition. This implies that a gradient in OH concentration in the CA  
362 particles is negligible under the current conditions.

#### 363 4. Discussion

364 Kessler et al. (Kessler et al., 2012) have reported the  $k_2$  of CA toward OH to be  
365  $(4.3 \pm 0.8) \times 10^{-13} cm^3 molecule s^{-1}$  at 308 K and 30 % RH with an Aerodyne HR-AMS.  
366 In their work, the diameter of particles and RH were equivalent to the current work,  
367 while their experimental temperature was 10 K higher. In addition, a m/z fragment of  
368 68 was used as a tracer for CA in their work to derive the heterogeneous rate constant.  
369 Conversely, no significant consumption of m/z 68 was observed in the current study.  
370 The lack of a m/z 68 fragment consumption here may be explained by the choice of  
371 reaction conditions. In the work of Kessler et al., OH concentration exposure  
372  $(0 \sim 7 \times 10^{12} molecule cm^{-3} s)$  was approximately an order of magnitude higher than that  
373 reported here. Recent evidence suggests that the product distribution during OA

374 oxidation greatly depends upon OH exposure levels (Wilson et al., 2012). Hence, it is  
375 possible that more oxidized products formed via multi-generational chemistry at high  
376 OH were formed, which may have less of an influence on the signal of the chosen  
377 tracer (m/z 68), and result in product AMS spectra which are significantly different  
378 than that of the reactant thus mitigating the use of PMF (which was not the case here).  
379 Secondly, a high resolution time-of-flight aerosol mass spectrometer (HR-ToF-AMS)  
380 was used in their work, while a C-ToF-AMS with unit-mass resolution was used in  
381 this study. The higher mass resolution of the HR-ToF-AMS relative to a C-ToF-AMS,  
382 may further reduce the influence of product fragments on m/z 68 (or others). Finally,  
383 differences in temperature or other reaction conditions between experiments may also  
384 have led to differences in the morphology of CA and subsequent differences in the  
385 reactivity of CA.

386       Given the above discrepancy in the consumption of m/z 68, the fragments at m/z  
387 129 and 147 were used as tracers in this work. The measured  $k_2$  of CA utilizing m/z  
388 129 and 147 in this study is of the same order of magnitude as that reported in Kessler  
389 et al. (2012). However, as shown in Figure 3C, the consumption of m/z 87 is much  
390 lower than that of m/z 129. The apparent  $k_2$  of CA based on m/z 87 is  $(9.9 \pm 0.8) \times 10^{-14}$   
391  $\text{cm}^3 \text{ molecule}^{-1} \text{ s}^{-1}$ , and the diffusion-corrected  $k_2$  is  $(1.16 \pm 0.09) \times 10^{-13} \text{ cm}^3 \text{ molecule}^{-1}$   
392  $\text{s}^{-1}$ . This suggests that the derived rate constant greatly depends upon the size of the  
393 tracer fragment, with larger fragments resulting in larger values of  $k_2$  in this study.  
394 This is consistent with previous work investigating the OH oxidation of tris-phenyl  
395 phosphate (TPhP) (Liu et al., 2014) and ambient biogenic SOA (Slowik et al., 2012).

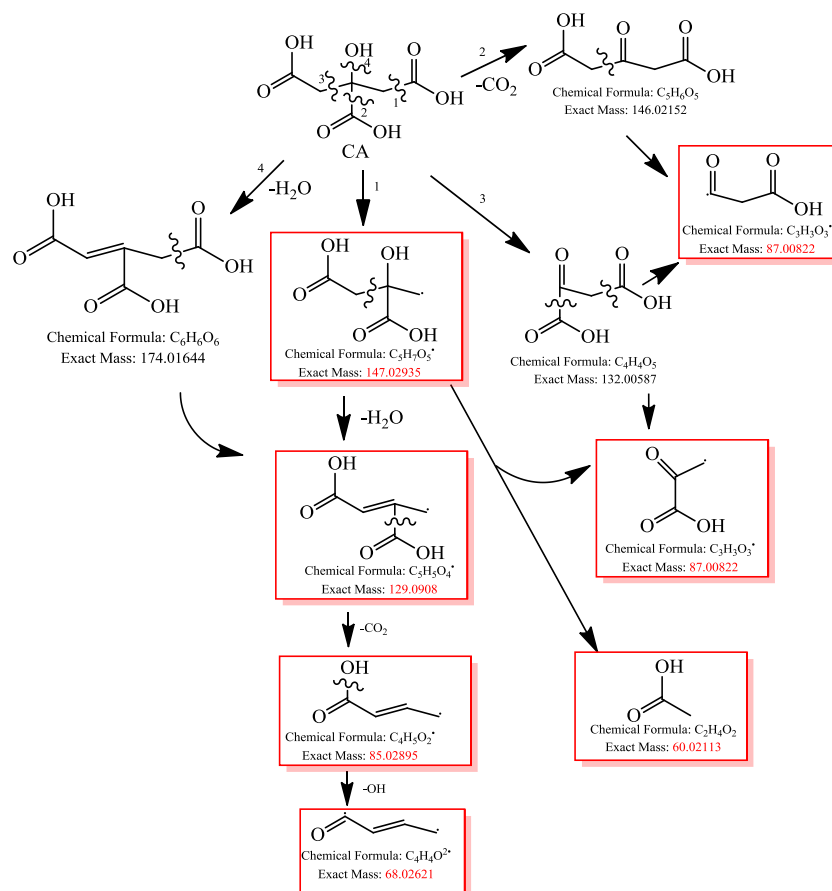
396 The  $k_2$  of CA based upon PMF analysis is approximately an order of magnitude larger  
397 than the Kessler result measured with the tracer at  $m/z$  68, and 4.2 times greater than  
398 that calculated based upon  $m/z$  147 in this study. The differences in product  
399 distributions that may arise between this and the work of Kessler et al., consistent  
400 with the fact that  $m/z$  68 is not consumed in the current study, suggests that; (1) the  
401 PMF approach was likely required in this work to separate similar product and  
402 reactant spectra ultimately caused by lower OH exposure, and (2) that the two derived  
403 rate constants are indeed different.

404 A number of factors may be responsible for the discrepancy between derived rate  
405 constants. It has previously been observed that the presence of  $O_3$  can inhibit the rate  
406 of OH reaction, perhaps by reacting with OH radicals or by  $O_3$  or intermediate species  
407 blocking surface active sites (Renbaum and Smith, 2011). A Langmuir-Hinshelwood  
408 mechanism has been observed for the reaction of  $O_3$  on organic surfaces (Pöschl,  
409 2005). It has also been demonstrated that a higher concentration of gas phase reactant  
410 often leads to a lower uptake coefficient due to surface saturation (Ma et al., 2010 ;Li  
411 et al., 2002). Differences in  $k_2$  may also arise from the competition between reaction  
412 products and reactants for available OH, or via the blocking or coating of the reactant  
413 by products which would require liquid phase diffusion of OH to degrade the original  
414 CA. In experiments with higher OH exposures (Kessler et al 2012) it is possible that  
415 significantly more product mass is mixed and/or coated onto the original particle thus  
416 decreasing the perceived  $k_2$ . Finally, as pointed out above, the differing reaction  
417 conditions may have led to a different CA morphology and subsequent differences in

418 the reactivity towards OH. The significant difference between the reported rate  
419 constants highlights an important issue in heterogeneous reactions of the atmosphere,  
420 and in the experiments trying to derive such kinetics. It implies that the particle  
421 composition and/or morphology as determined by the reaction conditions in the  
422 laboratory or the ambient atmosphere will have a large effect on the OH kinetics.

423 Citric acid is a hydroxyl substituted poly carboxyl acid. Scheme 1 summarizes its  
424 possible fragmentation pathways. The typical mass peaks including m/z 147, 129, 87,  
425 85 and 68 would result from this scheme and were indeed observed. The fragments at  
426 m/z 129, 87, 85 and 68 are also likely from CA oxidation products fragments, and  
427 hence their signal intensities may be highly influenced by products and/or larger  
428 fragments, **in particular, when the oxidized products are highly similar to the reactant.**  
429 In some instances, oxidation products can exhibit similar fragmentation pathways as  
430 the reactants. This is likely the case for the smaller fragments of CA. For example,  
431 scheme 2 illustrates the possible fragmentation pathways of  
432 2,3-dihydroxypropane-1,2,3-tricarboxylic acid, which is one of the products from the  
433 OH oxidation of citric acid (Atkinson, 1986). As observed in Scheme 2, there are  
434 several pathways leading to the fragment at m/z 87, implying that the decrease in the  
435 signal of m/z 87 due to CA oxidation is likely to be compensated by fragments from  
436 the oxidation products. In addition, it is also possible to form fragments with the same  
437 m/z as the parent citric acid if the dehydration reaction (the 6<sup>th</sup> path in Scheme 2)  
438 takes place initially. **This is highly possible when the product distribution contains**  
439 **products which are structurally similar to the reactant under low oxidant exposure**

440 conditions.

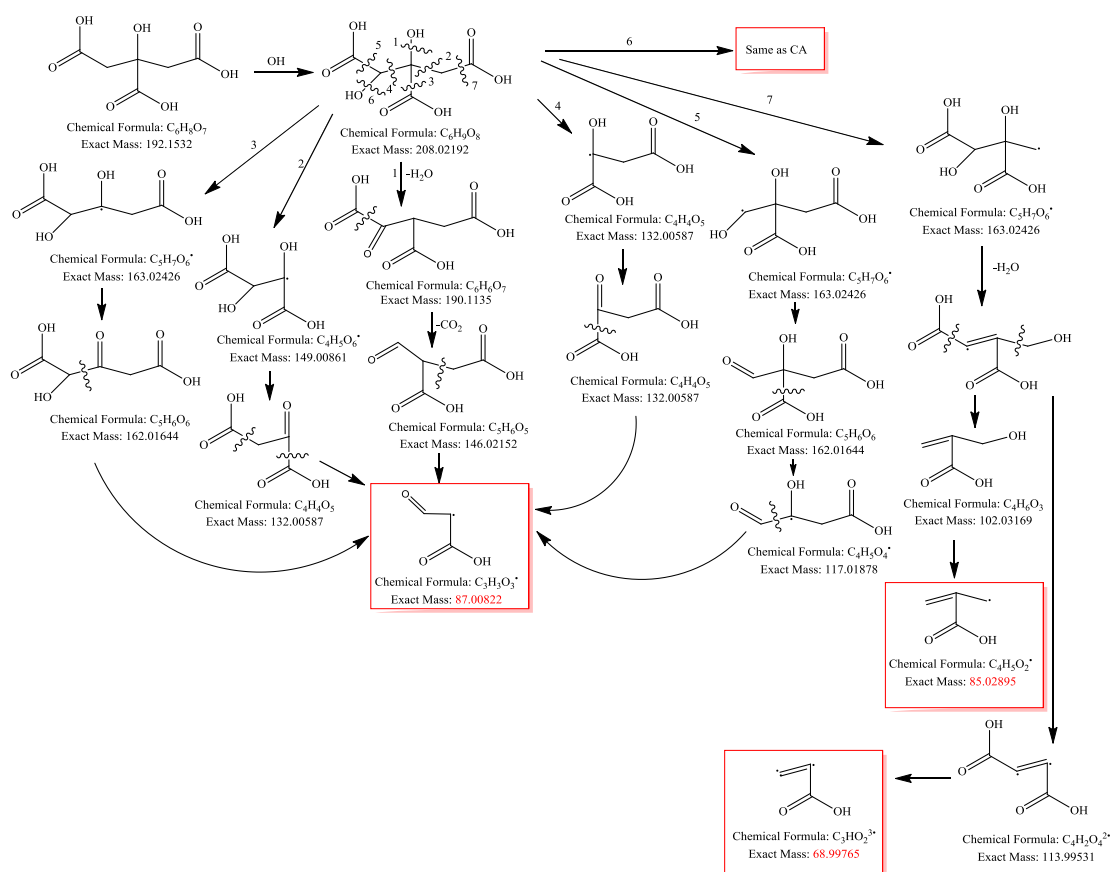


441

442

Scheme 1. Possible fragmentation pathways for citric acid.

443



444

445

446 Scheme 2. Possible fragmentation pathways for an oxidation product of citric acid.

447

448 The current relative rate method based upon PMF analysis was used to re-analyze  
 449 the heterogeneous oxidation kinetics of three organophosphate flame retardants found  
 450 in ambient particles and reported previously (Liu et al., 2014). The  $k_2$  values for TPhP,  
 451 tris-1,3-dichloro-2-propyl phosphate (TDCPP) and tris-2-ethylhexyl phosphate (TEHP)  
 452 utilizing the tracer and PMF approaches are summarized in Table 1. For TPhP, its  
 453 molecular ion peak ( $M^+$ ; 326) was chosen as a tracer; while the largest detectable  
 454 fragments, i.e.  $m/z$  381 and 323, were chosen for TDCPP ( $M^+$ ; 431) and TEHP ( $M^+$ ;  
 455 435), respectively. The typical evolution of the PMF factors of TPhP, TDCPP, and

456 TEHP are shown in Figures S1-3. For TPhP, the measured  $k_2$  values derived by both  
457 methods are comparable within the experimental uncertainties, while  $k_2$  of TDCPP  
458 and TEHP based upon PMF analysis is 1.5 and 1.6 times larger than that using the  
459 chosen tracers. The good agreement between methods for TPhP is likely due to the  
460 fact that the molecular ion peak ( $M^+$ ) is measurable for TPhP with the AMS, while it  
461 is not observable for TDCPP, TEHP and CA. Therefore, the influence of secondary  
462 fragmentation from larger fragments has little influence on the signal of  $M^+$  for TPhP.  
463 These results also demonstrate that a substantial underestimation of rate constants  
464 could result when a non-molecular ion tracer is used to monitor the particle phase  
465 concentration of organic matter with UMR-AMS for heterogeneous kinetic studies.  
466 The discrepancy between the tracer and PMF based methods for other compounds  
467 will depend upon a number of factors including: structure of products, OH exposure  
468 level, particle morphology, and organic species competing OH reactions.

469

## 470 **5.0 Implications and Conclusions**

471 An improvement in the mixed-phase relative rates technique is achieved based  
472 upon PMF analysis of UMR-AMS derived spectra. The measured  $k_2$  for citric acid  
473 toward OH is  $(3.31 \pm 0.29) \times 10^{-12} \text{ cm}^3 \text{ molecule}^{-1} \text{ s}^{-1}$  at 298 K and 30 % RH. This value  
474 is at least 4.2 times greater than that calculated on the basis of atypical tracer m/z 147  
475 or 7.7 times greater than the Kessler's value (Kessler et al. 2012). These results  
476 suggest that the heterogeneous kinetics of OA is substantially underestimated when a  
477 non-molecular ion peak is used as the tracer to measure the particle phase

478 concentration of OA. In model simulations, the reactive uptake coefficient of OH or  
479 other radicals, which are calculated based upon  $k_2$ , is an important parameter in  
480 evaluating the fate of OA during transport. The current results suggest that the lifetime  
481 of OA estimated in models due to heterogeneous oxidation might be overestimated for  
482 a reaction system where the products are highly similar to the reactant and the kinetic  
483 data are derived by individual non-molecular m/z tracers of OA. The results also  
484 suggest that it may be necessary to revisit the kinetic data of other organic aerosol  
485 components (and OH uptake coefficients) which have been derived using the relative  
486 rates technique (George et al., 2007; Lambe et al., 2007) based on UMR-AMS. Finally,  
487 these results imply that the heterogeneous oxidation of aerosols will be dependent  
488 upon a number of factors related to the reaction system, and that a single rate constant  
489 for one system cannot be universally applied under all conditions. Future work is thus  
490 required to elucidate the chemical and physical parameters which control the OH  
491 heterogeneous reaction kinetics and the associated need to apply PMF for a variety of  
492 chemical systems. This may be best accomplished through systematic application of  
493 the PMF approach to species with differing mass spectral characteristics, such as  
494 linear/branched alkanes, monocarboxylic acids and other oxygenates.

#### 495 **Supporting Information**

496 Supplementary material related to this article is available online at:

497

#### 498 **Acknowledgements**

499 This research was funded by the Chemicals Management Plan (CMP) and the Clean



500 Air Regulatory Agenda (CARA).

501 **Literature Cited:**

502 Allan, J. D., Jimenez, J. L., Williams, P. I., Alfarra, M. R., Bower, K. N., Jayne, J. T., Coe, H., and  
503 Worsnop, D. R.: Quantitative sampling using an Aerodyne aerosol mass spectrometer 1. Techniques of  
504 data interpretation and error analysis, *J. Geophys. Res.*, 108, 4090, 10.1029/2002jd002358, 2003.

505 Atkinson, R.: Kinetics and Mechanisms of the Gas-Phase Reactions of the Hydroxyl Radical with  
506 Organic Compounds under Atmospheric Conditions, *Chem. Rev.*, 85, 69-201, 1986.

507 Atkinson, R., and Arey, J.: Atmospheric Degradation of Volatile Organic Compounds, *Chem. Rev.*, 103,  
508 4605-4638, 2003.

509 Cappa, C. D., Che, D. L., Kessler, S. H., Kroll, J. H., and Wilson, K. R.: Variations in organic aerosol  
510 optical and hygroscopic properties upon heterogeneous OH oxidation, *J. Geophys. Res.*, 116, D15204,  
511 10.1029/2011jd015918, 2011.

512 Donahue, N. M., Robinson, A. L., Hartz, K. E. H., Sage, A. M., and Weitkamp, E. A.: Competitive  
513 oxidation in atmospheric aerosols: The case for relative kinetics, *Geophys. Res. Lett.*, 32, L16805,  
514 10.1029/2005gl022893, 2005.

515 Drewnick, F., Hings, S. S., DeCarlo, P., Jayne, J. T., Gonin, M., Fuhrer, K., Weimer, S., Jimenez, J. L.,  
516 Demerjian, K. L., Borrmann, S., and Worsnop, D. R.: A New Time-of-Flight Aerosol Mass  
517 Spectrometer (TOF-AMS)—Instrument Description and First Field Deployment, *Aerosol Sci. Technol.*,  
518 39, 637-658, 2005.

519 Fuchs, N. A., and Sutugin, A. G.: *Highly Dispersed Aerosols*, Butterworth-Heinemann, Newton, MA,  
520 1970.

521 George, I. J., Vlasenko, A., Slowik, J. G., Broekhuizen, K., and Abbatt, J. P. D.: Heterogeneous  
522 oxidation of saturated organic aerosols by hydroxyl radicals: uptake kinetics, condensed-phase products,  
523 and particle size change, *Atmos. Chem. Phys.*, 7, 4187-4201, 2007.

524 George, I. J., and Abbatt, J. P. D.: Chemical evolution of secondary organic aerosol from OH-initiated  
525 heterogeneous oxidation, *Atmos. Chem. Phys.*, 10, 5551-5563, 2010.

526 Hearn, J. D., and Smith, G. D.: A mixed-phase relative rates technique for measuring aerosol reaction  
527 kinetics, *Geophys. Res. Lett.*, 33, L17805, 10.1029/2006gl026963, 2006.

528 Huisman, A. J., Krieger, U. K., Zuend, A., Marcolli, C., and Peter, T.: Vapor pressures of substituted  
529 polycarboxylic acids are much lower than previously reported, *Atmos. Chem. Phys.*, 13, 6647-6662,  
530 2013.

531 Isaacman, G., Chan, A. W. H., Nah, T., Worton, D. R., Ruehl, C. R., Wilson, K. R., and Goldstein, A. H.:  
532 Heterogeneous OH Oxidation of Motor Oil Particles Causes Selective Depletion of Branched and Less  
533 Cyclic Hydrocarbons, *Environ. Sci. Technol.*, 46, 10632-10640, 2012.

534 Jacobson, M. Z.: *Fundamentals of Atmospheric Modeling*, Cambridge University Press, 2005.

535 Jayne, J. T., Leard, D. C., Zhang, X., Davidovits, P., Smith, K. A., Kolb, C. E., and Worsnop, D.:  
536 Development of an Aerosol Mass Spectrometer for Size and Composition Analysis of Submicron  
537 Particles, *Aerosol Sci. Technol.*, 33, 49-70, 2000.

538 Kessler, S. H., Smith, J. D., Che, D. L., Worsnop, D. R., Wilson, K. R., and Kroll, J. H.: Chemical  
539 Sinks of Organic Aerosol: Kinetics and Products of the Heterogeneous Oxidation of Erythritol and  
540 Levoglucosan, *Environ. Sci. Technol.*, 44, 7005-7010, 2010.

541 Kessler, S. H., Nah, T., Daumit, K. E., Smith, J. D., Leone, S. R., Kolb, C. E., Worsnop, D. R., Wilson,

542 K. R., and Kroll, J. H.: OH-Initiated Heterogeneous Aging of Highly Oxidized Organic Aerosol, *J. Phys.*  
543 *Chem. A*, 116, 6358-6365, 2012.

544 Kolb, C. E., Cox, R. A., Abbatt, J. P. D., Ammann, M., Davis, E. J., Donaldson, D. J., Garrett, B. C.,  
545 George, C., Griffiths, P. T., Hanson, D. R., Kulmala, M., McFiggans, G., Pöschl, U., Riipinen, I., Rossi,  
546 M. J., Rudich, Y., Wagner, P. E., Winkler, P. M., Worsnop, D. R., and Dowd, C. D. O.: An overview of  
547 current issues in the uptake of atmospheric trace gases by aerosols and clouds, *Atmos. Chem. Phys.*, 10,  
548 10561-10605, 2010.

549 Kroll, J. H., and Seinfeld, J. H.: Chemistry of secondary organic aerosol: Formation and evolution of  
550 low-volatility organics in the atmosphere, *Atmos. Environ.*, 42, 3593-3624, 2008.

551 Lambe, A. T., Zhang, J. Y., Sage, A. M., and Donahue, N. M.: Controlled OH radical production via  
552 ozone-alkene reactions for use in aerosol aging studies, *Environ. Sci. Technol.*, 41, 2357-2363, 2007.

553 Lambe, A. T., Miracolo, M. A., Hennigan, C. J., Robinson, A. L., and Donahue, N. M.: Effective Rate  
554 Constants and Uptake Coefficients for the Reactions of Organic Molecular Markers (n-Alkanes,  
555 Hopanes, and Steranes) in Motor Oil and Diesel Primary Organic Aerosols with Hydroxyl Radicals,  
556 *Environ. Sci. Technol.*, 43, 8794-8800, 2009.

557 Li, P., Al-Abadleh, H. A., and Grassian, V. H.: Measuring heterogeneous uptake coefficients of gases on  
558 solid particle surfaces with a Knudsen Cell reactor: complications due to surface saturation and gas  
559 diffusion into underlying layers., *J. Phys. Chem. A*, 106, 1210-1219, 2002.

560 Liggio, J., Li, S. M., Vlasenko, A., Sjostedt, S., Chang, R., Shantz, N., Abbatt, J., Slowik, J. G.,  
561 Bottenheim, J. W., Brickell, P. C., Stroud, C., and Leaitch, W. R.: Primary and secondary organic  
562 aerosols in urban air masses intercepted at a rural site, *J. Geophys. Res.*, 115, D21305, doi:  
563 10.21029/22010JD014426, 2010.

564 Liu, C., Zhang, P., Wang, Y., Yang, B., and Shu, J.: Heterogeneous Reactions of Particulate  
565 Methoxyphenols with NO<sub>3</sub> Radicals: Kinetics, Products, and Mechanisms, *Environ. Sci. Technol.*, 46,  
566 13262-13269, 2012.

567 Liu, Y., Liggio, J., Harner, T., Jantunen, L., Shoeib, M., and Li, S.-M.: Heterogeneous OH initiated  
568 oxidation: A possible explanation for the persistence of organophosphate flame retardants in air,  
569 *Environ. Sci. Technol.*, 48, 1041-1048, 2014.

570 Ma, J., Liu, Y., and He, H.: Degradation kinetics of anthracene by ozone on mineral oxides, *Atmos.*  
571 *Environ.*, 44, 4446-4453, 2010

572 McNeill, V. F., Wolfe, G. M., and Thornton, J. A.: The Oxidation of Oleate in Submicron Aqueous Salt  
573 Aerosols: Evidence of a Surface Process, *J. Phys. Chem. A*, 111, 1073-1083, 2007.

574 McNeill, V. F., Yatavelli, R. L. N., Thornton, J. A., Stipe, C. B., and Landgrebe, O.: Heterogeneous OH  
575 oxidation of palmitic acid in single component and internally mixed aerosol particles: vaporization and  
576 the role of particle phase, *Atmos. Chem. Phys.*, 8, 5465-5476, 2008.

577 Norris, G., and Vedantham, R.: EPA positive matrix factorization (PMF) 3.0 fundamentals & user guide,  
578 U.S. Environmental Protection Agency, [www.epa.gov](http://www.epa.gov), 2008.

579 Pöschl, U.: Atmospheric Aerosols: Composition, Transformation, Climate and Health Effects, *Angew.*  
580 *Chem. Int. Ed.*, 44, 7520-7540, 2005.

581 Paatero, P., and Tapper, U.: Positive matrix factorization: a nonnegative factor model with optimal  
582 utilization of error estimates of data values, *Environmetrics* 5, 111-126, 1994.

583 Paatero, P.: Least squares formulation of robust non - negative factor analysis, *Chemom. Intell. Lab.*  
584 *Syst.*, 37, 23-35, 1997.

585 Paatero, P., and Hopke, P. K.: Discarding or downweighting highnoise variables in factor analytic

586 models, *Anal. Chim. Acta*, 490, 277-289, 2003.

587 Pankow, J. F.: An absorption-model of gas-particle partitioning of organic compounds in the  
588 atmosphere, *Atmos. Environ.*, 28, 185-188, 1994.

589 Price, H. C., Murray, B. J., Mattsson, J., O'Sullivan, D., Wilson, T. W., Baustian, K. J., and Benning, L.  
590 G.: Quantifying water diffusion in high-viscosity and glassy aqueous solutions using a Raman isotope  
591 tracer method, *Atmos. Chem. Phys.*, 14, 3817-3830, 2014.

592 Reff, A., Eberly, S. I., and Bhave, P. V.: Receptor modeling of ambient particulate matter data using  
593 positive matrix factorization: Review of existing methods, *J. Air Waste Manage.*, 57, 146-154, 2007.

594 Renbaum, L. H., and Smith, G. D.: Artifacts in measuring aerosol uptake kinetics: the roles of time,  
595 concentration and adsorption, *Atmos. Chem. Phys.*, 11, 6881-6893, 2011.

596 Sareen, N., Moussa, S. G., and McNeill, V. F.: Photochemical Aging of Light-Absorbing Secondary  
597 Organic Aerosol Material, *J. Phys. Chem. A*, 117, 2987-2996, 2013.

598 Schwartz, R. E., Russell, L. M., Sjostedt, S. J., Vlasenko, A., Slowik, J. G., Abbatt, J. P. D., Macdonald,  
599 A. M., Li, -S. M., Liggio, J., Toom-Sauntry, D., and Leaitch, W. R.: Biogenic oxidized organic  
600 functional groups in aerosol particles from a mountain forest site and their similarities to laboratory  
601 chamber products, *Atmos. Chem. Phys.*, 10, 5075-5088, 2010.

602 Slowik, J. G., Wong, J. P. S., and Abbatt, J. P. D.: Real-time, controlled OH-initiated oxidation of  
603 biogenic secondary organic aerosol, *Atmos. Chem. Phys.*, 12, 9775-9790, 2012.

604 Smith, J. D., Kroll, J. H., Cappa, C. D., Che, D. L., Liu, C. L., Ahmed, M., Leone, S. R., Worsnop, D.  
605 R., and Wilson, K. R.: The heterogeneous reaction of hydroxyl radicals with sub-micron squalane  
606 particles: a model system for understanding the oxidative aging of ambient aerosols, *Atmos. Chem.  
607 Phys.*, 9, 3209-3222, 2009.

608 Song, Y., Zhang, Y., Xie, S., Zeng, L., Zheng, M., Salmon, L. G., Shao, M., and Slanina, S.: Source  
609 apportionment of PM<sub>2.5</sub> in Beijing by positive matrix factorization, *Atmos. Environ.*, 40, 1526-1537,  
610 2006.

611 Ulbrich, I. M., Canagaratna, M. R., Zhang, Q., Worsnop, D. R., and Jimenez, J. L.: Interpretation of  
612 organic components from Positive Matrix Factorization of aerosol mass spectrometric data, *Atmos.  
613 Chem. Phys.*, 9, 2891-2918, 2009.

614 Viana, M., Kuhlbusch, T. A. J., Querol, X., Alastuey, A., Harrison, R. M., Hopke, P. K., Winiwarter, W.,  
615 Vallius, A., Szidat, S., Prevot, A. S. H., Hueglin, C., Bloemen, H., Wahlin, P., Vecchi, R., Miranda, A. I.,  
616 Kasper-Giebl, A., Maenhaut, W., and Hitzenberger, R.: Source apportionment of particulate matter in  
617 Europe: A review of methods and results, *J. Aerosol. Sci.*, 39, 827-849, 2008.

618 Weitkamp, E. A., Hartz, K. E. H., Sage, A. M., Donahue, N. M., and Robinson, A. L.: Laboratory  
619 measurements of the heterogeneous oxidation of condensed-phase organic molecular makers for meat  
620 cooking emissions, *Environ. Sci. Technol.*, 42, 5177-5182, 2008a.

621 Weitkamp, E. A., Lambe, A. T., Donahue, N. M., and Robinson, A. L.: Laboratory Measurements of the  
622 Heterogeneous Oxidation of Condensed-Phase Organic Molecular Makers for Motor Vehicle Exhaust,  
623 *Environ. Sci. Technol.*, 42, 7950-7956, 2008b.

624 Widmann, J. F., and Davis, E. J.: Mathematical models of the uptake of ClONO<sub>2</sub> and other gases by  
625 atmospheric aerosols, *J. Aerosol. Sci.*, 28, 87-106, 1997.

626 Wilson, K. R., Smith, J. D., Kessler, S. H., and Kroll, J. H.: The statistical evolution of multiple  
627 generations of oxidation products in the photochemical aging of chemically reduced organic aerosol,  
628 *Phys. Chem. Chem. Phys.*, 14, 1468-1479, 2012.

629 Worsnop, D. R., Morris, J. W., Shi, Q., Davidovits, P., and Kolb, C. E.: A chemical kinetic model for

630 reactive transformations of aerosol particles, *Geophys. Res. Lett.*, 29, 1996, 10.1029/2002gl015542,  
631 2002.

632 Yuan, Z. B., Yu, J. Z., Lau, A. K. H., Louie, P. K. K., and Fung, J. C. H.: Application of positive matrix  
633 factorization in estimating aerosol secondary organic carbon in Hong Kong and its relationship with  
634 secondary sulfate, *Atmos. Chem. Phys.*, 6, 25-34, 2006.

635 Zhang, Q., Jimenez, J., Canagaratna, M., Ulbrich, I., Ng, N., Worsnop, D., and Sun, Y.: Understanding  
636 atmospheric organic aerosols via factor analysis of aerosol mass spectrometry: a review, *Anal. Bioanal.*  
637 *Chem.*, 401, 3045-3067, 2011.

638  
639  
640  
641  
642  
643  
644  
645  
646  
647  
648  
649  
650  
651  
652  
653  
654  
655  
656  
657  
658  
659  
660  
661  
662  
663  
664  
665  
666  
667  
668  
669  
670  
671  
672  
673

674 **Table 1.** Comparison of the measured  $k_2$  values utilizing PMF and select m/z tracers,

675 for organophosphate compounds and CA.

OA	Mean $k_{r\_PMF}$	$k_2 (10^{12}) \text{ cm}^3 \text{ molecule}^{-1} \text{ s}^{-1}$			$k_{2\_PMF}/$ $k_{2\_Tracer}$	$M_{Tracer}/M^+$
		$k_{2, \text{obs\_PMF}}$	$k_{2, \text{t\_PMF}}$	$k_{2, \text{t\_Tracer}}$		
TPhP	1.58±0.33	1.48±0.31	1.95±0.43	2.10±0.19 <sup>a</sup>	0.9	326/326
TDCPP	1.20±0.31	1.13±0.29	1.35±0.35	0.92±0.09 <sup>a</sup>	1.5	381/431
TEHP	3.52±0.65	3.31±0.61	4.25±0.78	2.70±0.63 <sup>a</sup>	1.6	323/435
CA	3.01±0.27	2.83±0.25	3.31±0.29	0.79±0.06	4.2	147/192

676 a.(Liu et al., 2014)

677

678

679

680

681

682

683

684

685

686

687

688

689

690

691

692

693 **Figure captions**

694 **Figure 1.** Changes in (A) total organic mass concentration, (B) the fraction of  
695 unreacted citric acid derived by PMF and (C) products of citric acid oxidized by OH  
696 derived by PMF, as a function of relative experimental time. The values 1 – 6  
697 represent a step-wise O<sub>3</sub> concentration decrease, corresponding to decreased OH  
698 exposure; 0 represents an O<sub>3</sub> concentration of zero. Experimental conditions are  $D_m$ :  
699 200 nm, RH:  $30 \pm 3$  %, T: 298 K.

700 **Figure 2.** Normalized mass spectra of (A) citric acid (PMF factor 1), (B) citric acid  
701 oxidation products (PMF factor 2), and (C) the difference mass spectrum (Factor 2 –  
702 Factor 1). The numbers in the upper two rows are the intensities of m/z 87 and 129,  
703 while negative values are shown in the bottom row. The red and green lines indicate a  
704 negative and positive value, respectively.

705 **Figure 3.** Mass spectra (A) of CA from NIST database, (B) of pure CA measured with  
706 the C-ToF-AMS.

707 **Figure 4.** Comparison between the mass spectra of factor 1 from PMF analysis and  
708 pure CA directly measured by the C-ToF-AMS. The inset graph is the correlation of  
709 their corresponding signal intensities.

710 **Figure 5.** Changes in the relative concentration of (A) methanol, (B) citric acid  
711 extracted with PMF analysis and (C) specific tracers measured with the AMS during  
712 the OH initiated oxidation of citric acid. Experimental conditions are  $D_m$ : 140 nm, RH:  
713  $30 \pm 3$  %, T: 298 K. The values in the top row represent the OH exposures.

714 **Figure 6.** Relative concentration of citric acid ( $c/c_0$ ) as a function of the relative  
715 concentration of methanol based upon (A) PMF analysis, (B) m/z=129 and (C) m/z

716 147. Experimental conditions are  $D_m$ : 140 nm, RH:  $30 \pm 3$  %, T: 298 K.

717

718

719

720

721

722

723

724

725

726

727

728

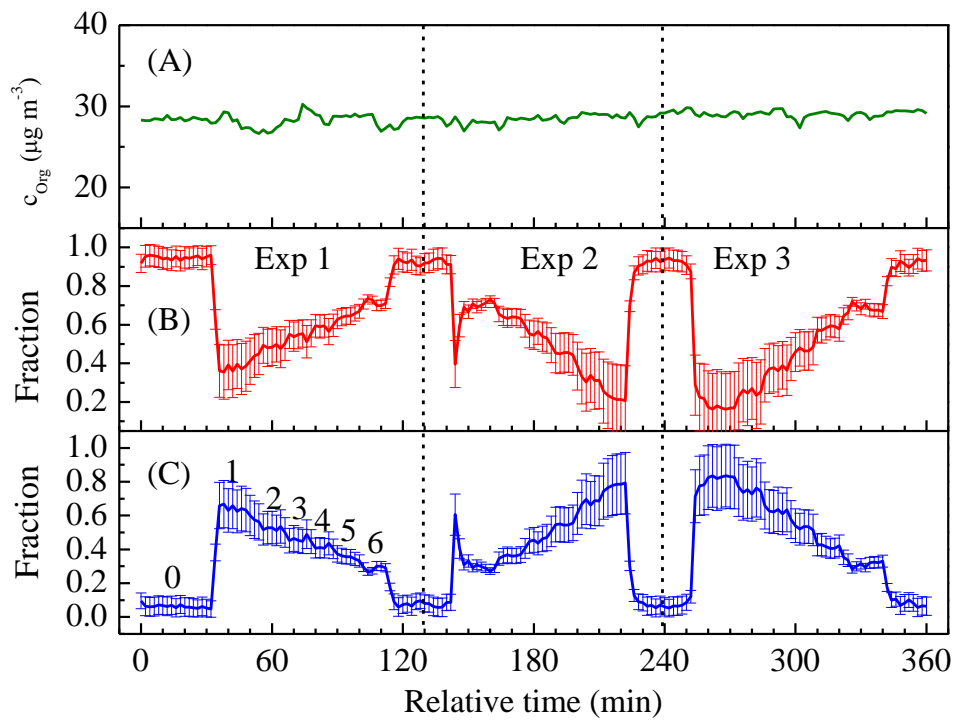


**Figure 1.**

729

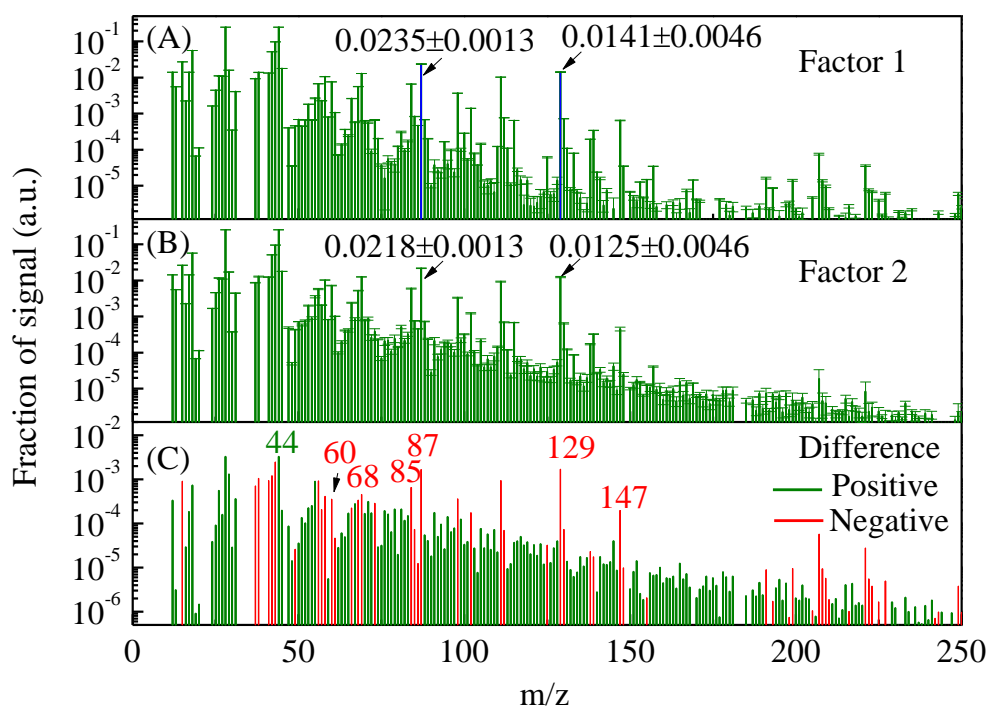
730

731

732

733





734

735

736

737

738

739

740

**Figure 2.**

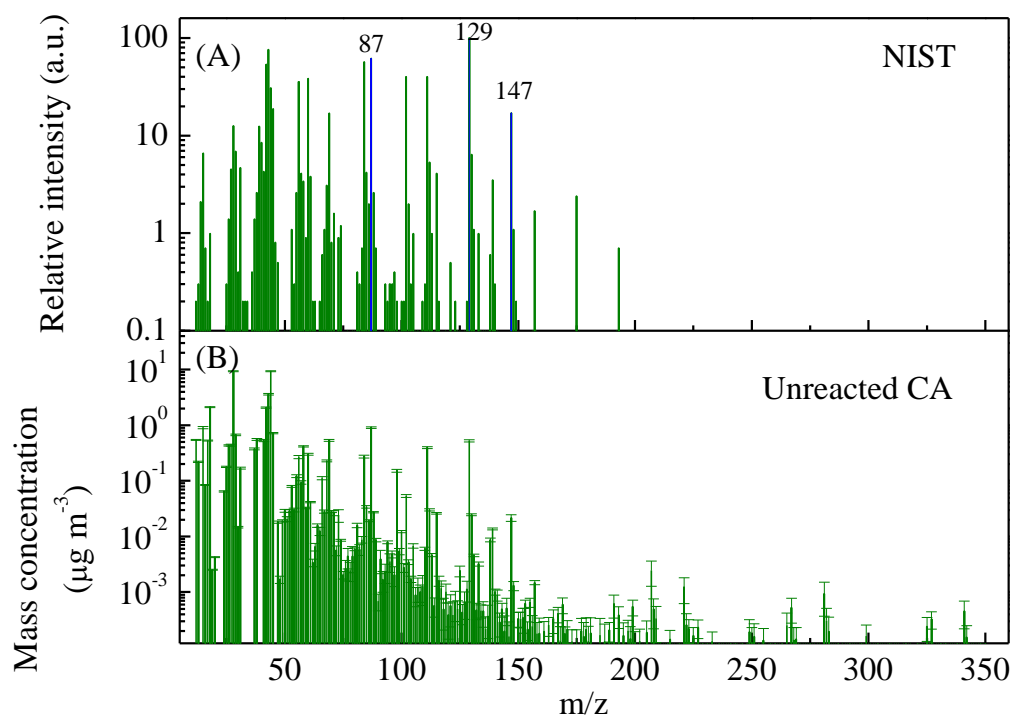


**Figure 3.**

741

742

743

744

745

746

747

748

749

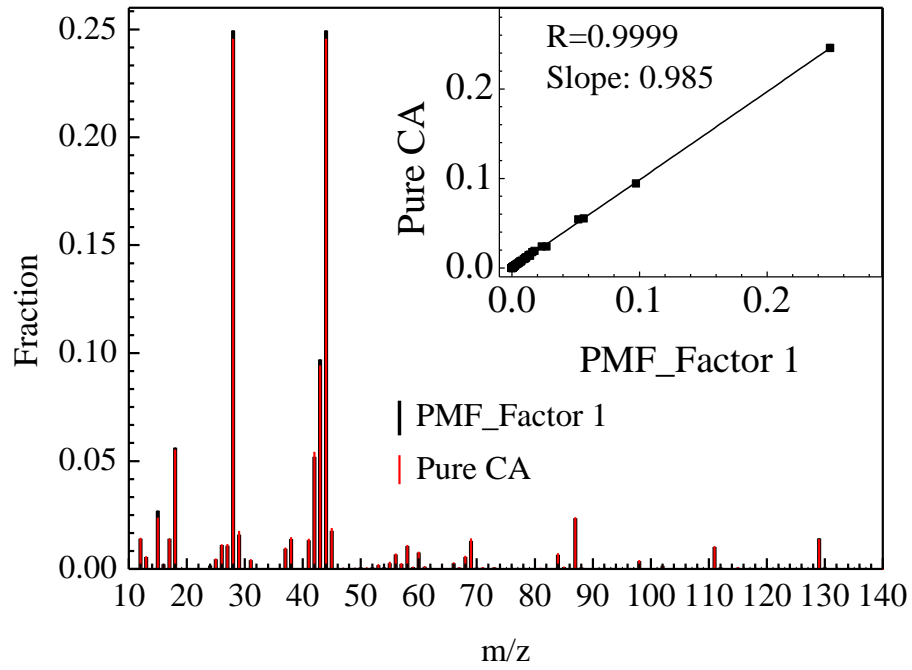
750

751

752

753

754



755

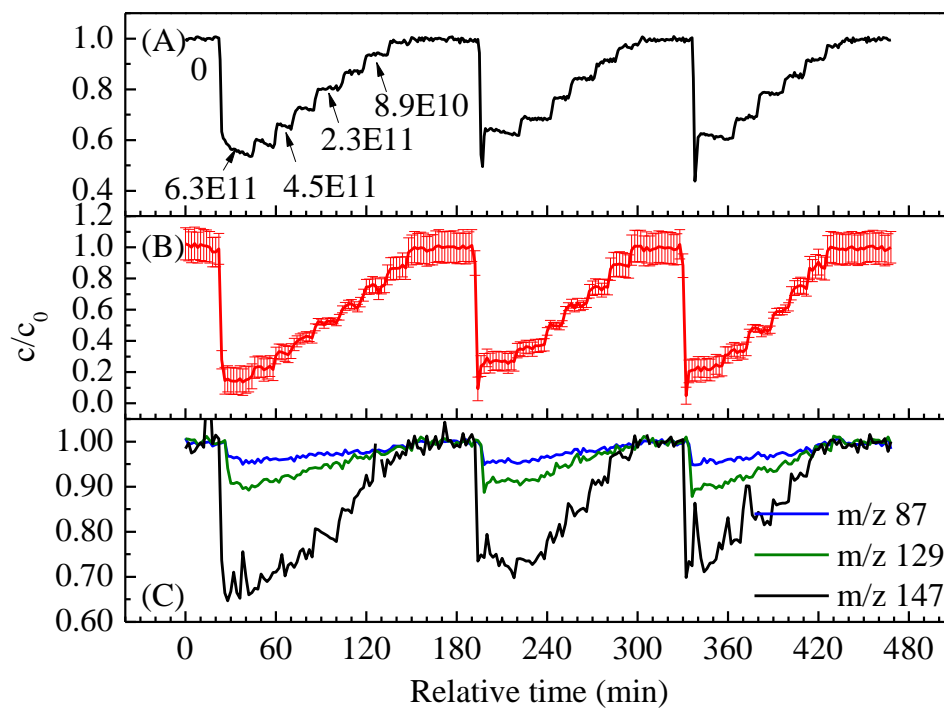
756

757

758

759

**Figure 4.**



760

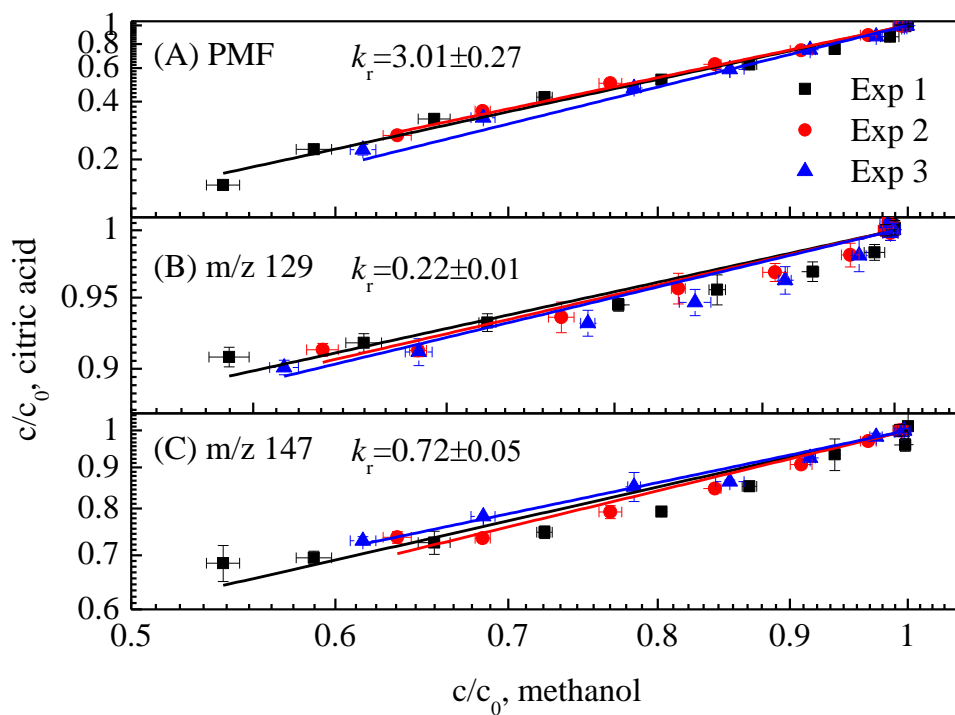
761

762

763

764

**Figure 5.**



765

766

767

**Figure 6.**